J. Fluid Mech. (1977), *vol.* 83, *part* 2, *pp.* 225–247
Printed in Great Britain

Experimental study of the stability of heated laminar boundary layers in water

By A. J. STRAZISAR, E. RESHOTKO AND J. M. PRAHL

Department of Fluid, Thermal, and Aerospace Sciences,
Case Western Reserve University, Cleveland, Ohio 44106

(Received 7 June 1976 and in revised form 5 April 1977)

Linear sinusoidal disturbances are introduced into the boundary layer over a heated flat plate of uniform surface temperature using a vibrating ribbon. The experiment is performed in a low turbulence water tunnel with free-stream turbulence intensities of 0·1–0·2 %. Measurements are made using temperature-compensated hot-film anemometry. Neutral-stability characteristics obtained for the unheated case agree favourably with previous results obtained both in water and in air. Neutral-stability and spatial disturbance-growth-rate characteristics measured for wall temperatures up to 8 °F above the free-stream temperature verify trends established by parallel-flow solutions of the disturbance momentum and energy equations. Disturbance growth rates and the band of amplified disturbance frequencies both decrease as wall heating is increased. The experimentally observed increase in the minimum critical Reynolds number $Re_{c\min}$ with increased wall heating agrees with the trend predicted by theory. However, effects of non-parallel flow act to reduce the measured values of $Re_{c\min}$ by about 120 units compared with predicted parallel-flow values independent of the level of wall heating.

1. Introduction

The instability of small amplitude disturbances in a laminar boundary layer is generally accepted as being a first step in the gradual process of transition to turbulent flow. For this reason many experimental and numerical investigations of boundary-layer stability have been undertaken in an attempt to develop a better understanding of this aspect of the transition process.

The first experimental study of flat-plate boundary-layer stability in air was by Schubauer & Skramstad (1948), who used hot-wire anemometry to measure the growth characteristics of sinusoidal velocity disturbances introduced into the boundary layer by a vibrating ribbon. Ross *et al.* (1970) repeated the Schubauer & Skramstad experiment to obtain data for comparison with improved numerical solutions of the Orr–Sommerfeld equation. Similar stability experiments have been performed in water by Wortmann (1955) and Nice (1973).

The results of the above experiments are in agreement with numerical solutions of the Orr–Sommerfeld equation except near the minimum critical Reynolds number, where the departure from parallel-flow theory seemingly results from the breakdown

of the parallel-flow assumption. Among the attempts to correct the parallel-flow formulation, those of Bouthier (1972, 1973) and Saric & Nayfeh (1975) yield numerical results which display the best agreement with experimental results. Both Bouthier and Saric & Nayfeh employ the method of multiple scales to include the effects of non-parallel flow.

A natural extension of the above work is the investigation of factors which can increase boundary-layer stability. One of these factors is wall heating in water, which yields a velocity profile that is more stable than the Blasius profile owing to the temperature dependence of viscosity through the boundary layer.

The first numerical results on the spatial stability of heated water boundary layers were obtained by Wazzan, Okamura & Smith (1968, 1970). Lowell (1974) reformulated the problem, including all fluid-property variations in the boundary layer along with the disturbance energy equation, thereby predicting fluid-property fluctuations as well as temperature fluctuations in the boundary layer.

The objective of the present investigation is to find out whether the increased stability predicted by the results of Wazzan *et al.* (1970) and Lowell (1974) is in fact realized. To this end the stability of the flat-plate boundary layer is investigated on both a heated and an unheated plate using temperature-compensated hot-film anemometry to measure the growth rates of artificial disturbances introduced into the boundary layer by a vibrating ribbon.

Experimental results obtained in the unheated boundary layer are compared with numerical results from both the parallel- and the non-parallel-flow formulations of Saric & Nayfeh (1975). Experimental results in the heated boundary layer are compared with those in the unheated layer to verify trends predicted by the numerical results of Lowell (1974).

2. Notation

In this paper bars are placed over dimensional variables when they appear alone, but are dropped when the variables are dimensionless or appear as part of a dimensionless group. The x co-ordinate is measured along the length of the plate downstream from the leading edge, the y co-ordinate is measured normal to the plate surface and the transverse (spanwise) co-ordinate z is measured from the plate centre-line.

The dimensional mean-flow quantities are $\bar{x}$, $\bar{y}$, $\bar{U}$ and $\bar{T}-\bar{T}_\infty$, where $\bar{U}$ is the local mean velocity in the boundary layer and $\bar{T}-\bar{T}_\infty$ is the difference between the local fluid temperature $\bar{T}$ in the boundary layer and the free-stream fluid temperature $\bar{T}_\infty$. The mean-flow reference quantities are $\bar{U}_e$ and $\bar{T}_w-\bar{T}_\infty$, where $\bar{U}_e$ is the local mean velocity at the outer edge of the boundary layer and $\bar{T}_w$ is the plate surface temperature. The level of wall heating is denoted by $\bar{T}_w-\bar{T}_\infty \pm \bar{\sigma}_T$, where $\bar{\sigma}_T$ is the standard deviation in the readings of eleven thermistors which measure the plate surface temperature. Values of $\bar{\sigma}_T$ found in the figure legends below are typical of those measured throughout the present work. The largest value of σ_T encountered is 8·5 %; the value is usually between 5 % and 7 %. In all cases the local surface temperature varies randomly about the mean, displaying no specific gradients. The non-dimensional mean-flow variables are $\eta = y(U_e/\nu_\infty x)^{\frac{1}{2}}$, u/U_∞, $(T-T_\infty)/(T_w-T_\infty)$ and the Reynolds number

$Re = U_e\delta^*/\nu_\infty$, where ν_∞ is the kinematic viscosity evaluated at the free-stream temperature and

$$\bar{\delta}^* = \left(\frac{\bar{\nu}_\infty \bar{x}}{\bar{U}_e}\right)^{\frac{1}{2}} \int_0^\infty \left(1 - \frac{U}{U_e}\right) d\eta.\dagger$$

The dimensional disturbance quantities are $\bar{u}'$, $\bar{T}'$, $\bar{f}$ and $\bar{\lambda}$, where $\bar{u}'$ and $\bar{T}'$ are the r.m.s. amplitudes of the fluctuating components of the axial velocity and temperature generated by the vibrating ribbon, $\bar{f}$ is the disturbance frequency and $\bar{\lambda}$ is the disturbance wavelength. The non-dimensional disturbance parameters are the disturbance velocity u'/U_e, the disturbance temperature $T'/(T_w - T_\infty)$, the wavenumber $\alpha_r = 2\pi\delta^*/\lambda$, the frequency $\omega_r = 2\pi f \nu_\infty/U_e^2$, the phase speed $c_r = \mathrm{Re}\,(\omega_r/\alpha_r)$, the group velocity $c_g = \mathrm{Re}\,(\partial\omega_r/\partial\alpha_r)$ and the spatial growth rate

$$-\alpha_i = \frac{1}{\bar{A}} \frac{d\bar{A}}{dx} \frac{\delta^*}{Re},$$

where $\bar{A}$ is the maximum value of $\bar{u}'(\eta)$ at a fixed $\bar{x}$.

3. Equipment and procedure

3.1. *The experimental facility*

The experiment is performed in a closed-circuit low turbulence water tunnel which has a test section 15·5 in. long, 9 in. wide and 6 in. high. The main turbulence reduction mechanisms in the tunnel are a settling chamber which contains 13 fine-mesh stainless-steel screens (100 wires/in., solidity = 0·28) and a 25 : 1 area contraction nozzle located between the settling chamber and the test section. The x component of the turbulence intensity in the test section is $I = 0{\cdot}1$–$0{\cdot}2$ % for $\bar{U}_e < 11$ ft/s. A heat exchanger built into the tunnel circuit is used to control free-stream temperature drift. Since boundary-layer stability characteristics are quite sensitive to the temperature difference $\bar{T}_w - \bar{T}_\infty$, stability measurements are discontinued whenever the drift in $\bar{T}_\infty$ exceeds 0·2 °F during a run.

The flat aluminium test plate, which is 13·6 in. long, 9 in. wide and 0·625 in. thick, is suspended from a frame which fits the top of the test section, as shown in figure 1.‡ The leading edge of the plate is located 0·425 in. below the top of the test section, thus forming a slot which spans the roof of the test section. The turbulent wall boundary layer in the water tunnel is removed through this slot by suction. The amount of suction is adjusted so as to locate the flow stagnation point at a stable

† For heated cases the use of a modified Howarth–Dorodnitsyn transformation yields

$$\eta = \left(\frac{U_e}{\nu_\infty x}\right)^{\frac{1}{2}} \int_0^\infty \frac{\rho}{\rho_e}\, dy, \quad \bar{\delta}^* = \left(\frac{\bar{\nu}_\infty \bar{x}}{\bar{U}_e}\right)^{\frac{1}{2}} \int_0^\infty \left(\frac{\rho_e}{\rho} - \frac{U}{U_e}\right) d\eta.$$

However, since the maximum value of $\bar{T}_w - \bar{T}_\infty$ used in the present work is 8 °F, for which $\rho_e/\rho_w - 1 = 2{\cdot}8 \times 10^{-4}$, the incompressible formulae given above are used to calculate δ^* and η for both heated and unheated cases.

‡ This mounting configuration results in the fluid being heated from above, which is an inherently stabilizing effect. However, Schlichting (1968, p. 492) has shown that laminar boundary-layer stability is not increased by buoyancy effects until the Richardson number is $Ri \sim 5 \times 10^{-3}$. Since the largest Richardson number encountered in the present work is $Ri = 3 \times 10^{-5}$, the increased boundary-layer stability observed in this work is not due to buoyancy effects.

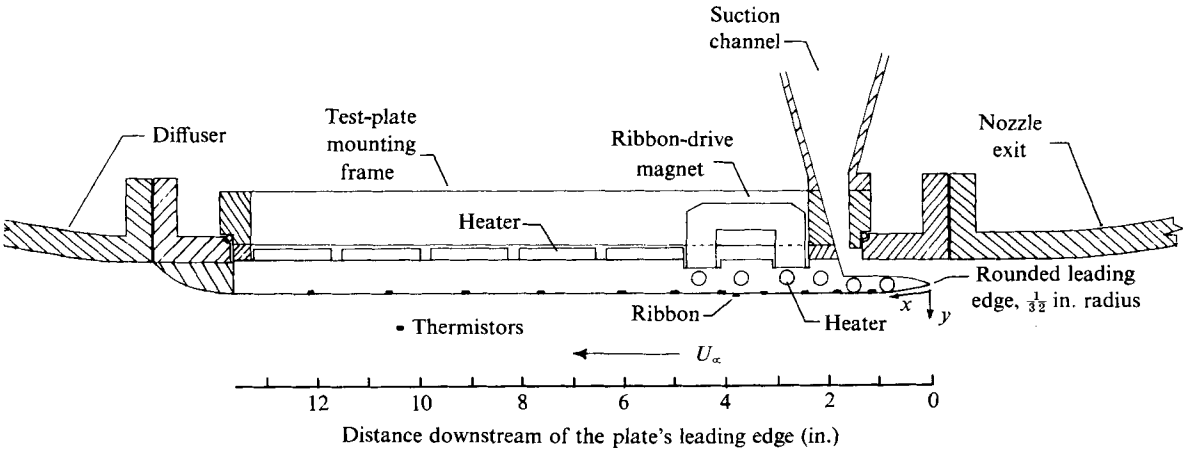

FIGURE 1. Sectional view of the plate as mounted in the test section.

position just downstream of the rounded leading edge (0·031 in. radius) on the test side of the plate. The position of the stagnation streamline is observed by means of dye injected upstream of the plate's leading edge and a static pressure tap located on the leading edge of the plate. A laminar boundary layer then develops along the plate starting from the stagnation point.

Plate heating is provided by eleven electric heating elements distributed along the plate as shown in figure 1. Streamwise uniformity of the plate surface temperature is checked by eleven thermistors imbedded in the plate surface along the centre-line. Spanwise uniformity of the surface temperature is checked by a spanwise array of five thermistors at $x = 6{\cdot}1$ in.

The pressure distribution along the plate is measured using static pressure holes located in the plate surface. Two static holes are located at each x position where the pressure is measured, each hole being located 1·5 in. off the plate centre-line, with the measured pressure taken as the average of that measured by each hole. At $x = 6{\cdot}38$ in. five static holes are located in a spanwise array. The pattern of static holes thus allows measurement of both the spanwise and the streamwise pressure distribution.

Artificial velocity disturbances are introduced into the boundary layer by a phosphor-bronze ribbon 0·001 in. thick and 0·125 in. wide which is stretched across the plate surface 3·75 in. behind the leading edge. Ribbon vibration is achieved by passing a sinusoidal current through the ribbon in the z direction in the presence of a magnetic field maintained by horseshoe magnets located on top of the plate. The ribbon is taped directly to the plate surface except for the central 2·5 in. to prevent ribbon flutter caused by the mean flow. A d.c. bias is added to the a.c. ribbon signal in order to lift the ribbon away from the plate so that it can vibrate without striking the plate. The position of the ribbon relative to the plate surface is unknown while the ribbon is vibrating. However, the important characteristics of the vibrating ribbon are the strength and purity of the velocity disturbance which it introduces into the boundary layer. These features are quite adequate in the present case as discussed in § 5 below.

The traversing mechanism used to position the anemometer probes provides

position control to within 0·001 in. in the x and y directions. The z position of the mechanism is fixed at the plate centre-line.

All velocity and temperature measurements reported here are performed along the plate centre-line. The spanwise arrays of thermistors and static pressure holes indicate no spanwise gradients in surface temperature or static pressure at the plate centre-line. Possible effects at the centre-line of corner interference between the test plate and the tunnel side walls could not be detected.

Further details concerning the experimental facility may be found in Strazisar (1975).

3.2. *Instrumentation*

The free-stream velocity is measured with a $\frac{3}{16}$ in. diameter Prandtl-type Pitot–static tube in conjunction with a manometer board capable of resolving pressure differences of 0·05 in. of water.

Temperatures in the plate and in the free stream are measured with thermistors and a thermistor thermometer with a resolution of 0·02 °F. Temperature measurements in the thermal boundary layer are made with a DISA 55D01 anemometer and a DISA 55F19 hot-film boundary-layer probe operated in the constant-current mode as a resistance thermometer. At the values of gain used in the present work the resolution of the resistance thermometer is also 0·02 °F.

Velocity measurements in the heated boundary layer are made with a DISA 55M01 constant-temperature anemometer equipped with a DISA 55M14 temperature-compensated bridge. A General Radio 1900-A wave analyser is used to measure the r.m.s. amplitude of the anemometer signal resulting from ribbon-generated disturbances in the boundary layer. Using a filter bandwidth of 3 Hz, signal-to-noise ratios of 10–20 are obtainable while keeping the peak disturbance amplitude $(u'/U_e)_{\max}$ below 1·5 %. The ribbon frequency is measured on a Hewlett–Packard 521c counter. Velocity spectrum measurements are made with a Singer LP-1a scanning spectrum analyser.

3.3. *Experimental procedure*

Temperature calibration of the anemometer as a resistance thermometer is performed using the free-stream temperature measured by thermistors extending 1 in. into the free stream through the side walls of the test section. The anemometer is calibrated for velocity against the Pitot–static tube located in the centre of the test section.

Velocity measurements with a hot-film anemometer are known to be very sensitive to changes in ambient temperature (Tan-atichat, Nagib & Pluister 1973). Therefore, before making velocity measurements in the heated boundary layer, proper operation of the temperature-compensation network is checked using the following procedure. The hot-film probe is placed near the wall ($\eta \approx 0{\cdot}5$) in the unheated boundary layer and the degree of temperature compensation is adjusted until the anemometer output voltage is unchanged when heat is applied to the plate. As a further check, velocity profiles taken in the heated and unheated boundary layer under identical free-stream flow conditions are compared with one another. Heated and unheated profiles should be identical within experimental error since Lowell's (1974) solutions indicate that changes in the mean velocity profile are less than the experimental measurement errors for the range of wall temperatures used here.

The boundary-layer displacement thickness $\bar{\delta}^*$ is calculated by plotting the mean velocity profile and performing the integration

$$\bar{\delta}^* = \left(\frac{\bar{\nu}_\infty \bar{x}}{\bar{U}_e}\right)^{\frac{1}{2}} \int_0^\infty \left(1 - \frac{U}{U_e}\right) d\eta$$

graphically using a polar planimeter. The Reynolds number $Re = U_e \delta^*/\nu_\infty$ is then formed using the kinematic viscosity evaluated at the free-stream temperature. Since $\bar{\delta}^*$ represents some measure of pressure-gradient history and wall heating effects on the mean velocity profile, use of the measured Re in data analysis is felt to be more accurate than the use of an Re calculated by assuming a Blasius mean velocity profile, i.e. $Re = 1{\cdot}7208(U_e x/\nu_\infty)^{\frac{1}{2}}$.

At a given Reynolds number, for each frequency, the disturbance amplitude is measured at five stations spaced 0·25 in. apart between $\bar{x} = 5$ in. and $\bar{x} = 6$ in. The Reynolds number is based on $\bar{\delta}^*$ measured at $\bar{x} = 5{\cdot}5$ in. Since the disturbance amplitude distribution in the boundary layer is not known *a priori*, the amplitude recorded at each x station is the peak amplitude, defined as $A(\bar{x}) = (u'(\eta, \bar{x})/U_e)_{\max}$, found by searching through the boundary layer. The spatial disturbance growth rate for that frequency and Reynolds number is then calculated from a least-squares polynomial curve fit of the $A(\bar{x})$ data. The growth rates so obtained for several frequencies at the same Reynolds number are plotted as shown in figure 7, where the error flags on each measured point represent the maximum uncertainty due to reading errors. Pairs of neutral points are then found from the $\alpha_i = 0$ intercepts of a smooth curve fitted through the α_i, ω_r plot. Near the minimum critical Reynolds number, points of neutral amplification are determined from points of zero slope on the curves fitted through the measured distribution of $A(\bar{x})$ taken at constant frequency.

The procedure of searching in the y direction for $(u'/U_e)_{\max}$ differs from the procedure used by previous investigators. Schubauer & Skramstad (1948) traversed in the x direction at a constant $\bar{y}$ while Ross *et al.* (1970) traversed in the x direction at a constant η. In both cases empirical corrections were added to the measured amplitudes to account for changes in the shape of the amplitude distribution between different x locations. The present method requires slightly more experimental effort but eliminates the need for empirical corrections of measured disturbance amplitudes and helps to minimize the ambiguities which can arise (as pointed out by Gaster 1974; Saric & Nayfeh 1975) when comparing experimental results with theoretical results.

The disturbance wavelength is measured using an oscilloscope. A reference signal from the ribbon is displayed on the upper trace while the hot-film anemometer output is displayed on the lower trace. The anemometer probes are traversed in the x direction at constant U/U_e until a 360° phase shift occurs between the anemometer output signal and the ribbon reference signal. The distance moved during this phase shift is one disturbance wavelength $\bar{\lambda}$. The wavelength measurement is made near $\bar{x} = 5{\cdot}5$ in. and the wavenumber α_r is then formed using the value of $\bar{\delta}^*$ measured at $\bar{x} = 5{\cdot}5$ in. Once the dispersion relation ω_r *vs.* α_r is known at a fixed Re, the neutral disturbance wavenumbers can be found from the neutral disturbance frequencies. Complete results for α_i *vs.* ω_r and α_r *vs.* ω_r as functions of Re and $\bar{T}_w - \bar{T}_\infty$ obtained using the above procedure appear in Strazisar (1975).

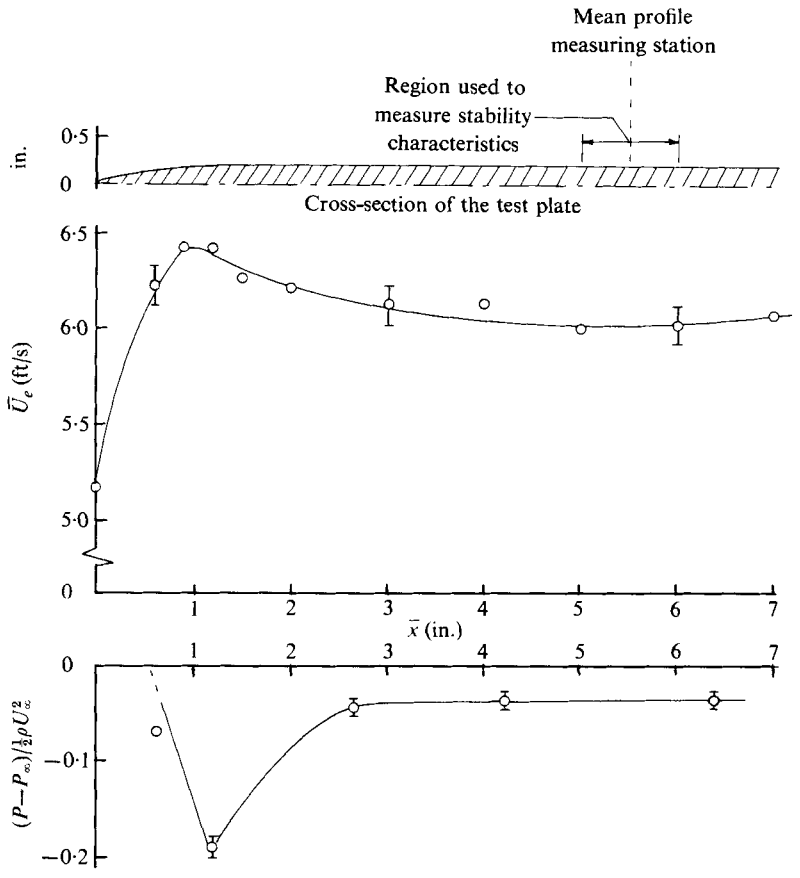

FIGURE 2. Typical static pressure and free-stream velocity distribution along the test plate.

4. The mean flow field

A typical free-stream velocity distribution measured with the hot-film anemometer and the corresponding static pressure distribution along the plate surface are shown in figure 2, along with a cross-sectional view of the test plate. The reference quantities $\bar{U}_\infty$ and $\bar{\rho}_\infty$ are measured at $\bar{x} = 0$. The pressure falls from the stagnation point at $\bar{x} = 0$ to a minimum in the vicinity of the shoulder between the tapered leading edge and the flat surface of the plate, while the velocity at the outer edge of the boundary layer reaches a maximum near the shoulder. The local Falkner–Skan parameter β is evaluated at $\bar{x} = 5{\cdot}5$ in. using the maximum uncertainty in static pressure measured at $\bar{x} = 4{\cdot}33$ in. and 6·38 in. For the case shown here the value is $\beta = (0{\cdot}4 \pm 3) \times 10^{-3}$. The maximum absolute value of β encountered in the present work is $|\beta| = 0{\cdot}02$.

The error flags shown in figure 2 and all following figures indicate the maximum uncertainty due to reading errors. Since the uncertainty in a non-dimensional parameter is generally a function of the magnitude of the parameter, error flags are placed on selected points over a range in parameter magnitudes to indicate the variations in uncertainty. Thus the absence of an error flag on a particular data point does not imply that the point is free of error.

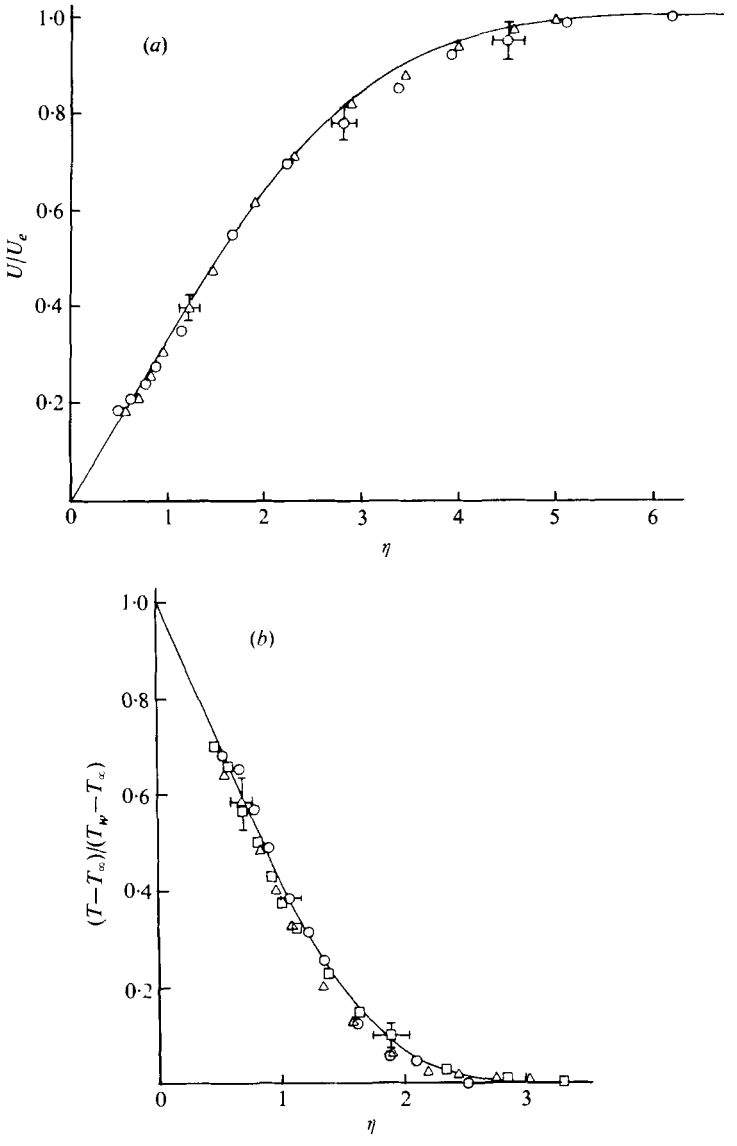

FIGURE 3. Typical mean velocity and temperature profiles. (*a*) ——, solution by Lowell (1974) for $\bar{T}_w - \bar{T}_\infty = 0\,°\text{F}$, $\beta = -3{\cdot}6 \times 10^{-3}$. Data: ○, $\bar{T}_w - \bar{T}_\infty = 0\,°\text{F}$, $\bar{T}_\infty = 75\,°\text{F}$, $Re = 940$; △, $\bar{T}_w - \bar{T}_\infty = 7{\cdot}82 \pm 0{\cdot}48\,°\text{F}$, $Re = 909$. (*b*) ——, solution by Lowell (1974) for $\bar{T}_w - \bar{T}_\infty = 5\,°\text{F}$, $\bar{T}_\infty = 75\,°\text{F}$, $\beta = 0$. Data: □, $\bar{T}_w - \bar{T}_\infty = 3{\cdot}48 \pm 0{\cdot}19\,°\text{F}$, $Re = 863$; ○, $\bar{T}_w - \bar{T}_\infty = 5{\cdot}40 \pm 0{\cdot}35\,°\text{F}$, $Re = 910$; △, $\bar{T}_w - \bar{T}_\infty = 7{\cdot}82 \pm 0{\cdot}48\,°\text{F}$, $Re = 909$.

Figure 3(*a*) compares heated and unheated mean velocity profiles measured under identical flow conditions with the calculated profile obtained with Lowell's (1974) program for $\beta = 3{\cdot}6 \times 10^{-3}$, which is the β measured for that particular case. For $\eta > 6$ the measured velocity is uniform to within 1 %. The thickness of the unheated boundary layer in the present case is $\bar{\delta} = 0{\cdot}066$ in. ($\eta = 6{\cdot}3$). The range of $\bar{\delta}$ encountered in the present work is $0{\cdot}057\,\text{in.} < \bar{\delta} < 0{\cdot}112\,\text{in.}$ Note that velocities measured in the region $\eta < 0{\cdot}75$ are consistently higher than would be expected from the straight-line

nature of the velocity profile in this region. These velocities may be subject to wall interference effects due to the size of the hot-film probe relative to the boundary layer. At the last measured point, $\eta \approx 0{\cdot}5$, the prongs of the hot-film probe touch the wall. The probe-prong diameter is 0·010 in. ($\eta = 0{\cdot}95$ in the present case), while the sensing-element diameter is 0·003 in. ($\eta = 0{\cdot}29$).

The discrepancy shown in figure 3(*a*) between measured and calculated velocity profiles for $\overline{T}_w - \overline{T}_\infty = 0$ may be due to the integrated effect of the upstream pressure distribution on the measured profile. The average value of $\delta^*/(\nu_\infty/U_e)^{\frac{1}{2}}$ for 55 mean profiles measured during the present investigation is 1·795, which is 4 % above the Blasius value of 1·7208. Note, as mentioned in § 3.3, that the difference between the heated and unheated velocity profiles is within experimental error. The heated profile is slightly fuller than the unheated profile in agreement with Lowell's (1974) numerical solutions of the variable-fluid-property boundary-layer equation. The calculated ratio of the values of δ^* for the heated and unheated boundary layers for this case is 0·968 while the measured ratio is 0·967.

Mean temperature profiles measured at various values of $\overline{T}_w - \overline{T}_\infty$ and Re are compared with Lowell's (1974) solution of the boundary-layer energy equation in figure 3(*b*). Note that the thickness of the thermal boundary layer is smaller than that of the velocity boundary layer, their ratio being approximately $\delta_T/\delta_u = Pr^{-\frac{1}{3}} = 0{\cdot}54$, where the Prandtl number of water is taken as 6·3 at $\overline{T}_\infty = 75\ ^\circ\mathrm{F}$. Further details concerning the mean flow field may be found in Strazisar (1975).

5. The disturbance flow field

One of the basic requirements for the experimental study of laminar boundary-layer stability is free-stream flow which is free of high natural disturbance levels. The free-stream turbulence intensity of the facility used in the present investigation is 0·1–0·2 % compared with 0·02–0·03 % for the facilities used by Schubauer & Skramstad (1948) and by Ross *et al.* (1970).

In view of the relatively high disturbance levels present in the water tunnel, velocity spectra are taken to investigate the strength and spectral quality of the ribbon-generated disturbance velocity. Figure 4 shows spectra taken under identical mean-flow conditions with and without an artificial disturbance present at 19·7 Hz. Also shown is the band of disturbance frequencies which receive amplification as predicted by the analysis for non-parallel flow of Saric & Nayfeh (1975). Note that the artificial disturbance falls within the band of amplified frequencies. The width of the peak centred at 19·7 Hz is to some extent a function of the spectrum analyser resolution rather than a true measure of the harmonic content of the artificial disturbance. In accordance with the assumptions of linear stability theory the artificial disturbance is orthogonal with respect to the natural disturbances in the boundary layer, i.e. the velocity amplitude at frequencies other than the ribbon frequency is not affected by the presence of the ribbon-generated disturbance. Another assumption of the linear theory is that the disturbance growth rate is independent of the disturbance amplitude. Linearity of the artificial disturbance is periodically checked over the range of flow conditions encountered in the present work by measuring the ribbon-generated disturbance growth rate under identical flow conditions at several different disturbance amplitudes. The results indicate that the growth rate is independent of the amplitude

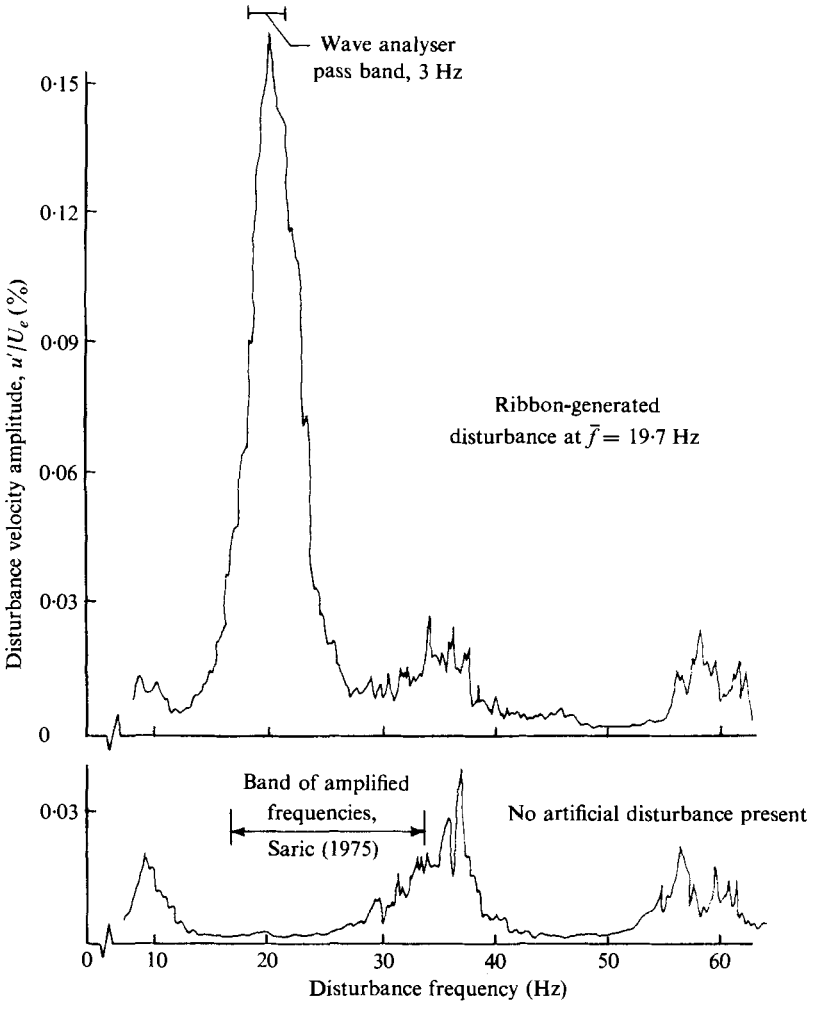

FIGURE 4. Spectral characteristics of the boundary layer with and without an artificial velocity disturbance present. $\bar{T}_w - \bar{T}_\infty = 0$ °F, $Re = 630$, $\eta = 0{\cdot}455$, $\bar{f} = 19{\cdot}7$ Hz, $\omega_r \times 10^6 = 141$.

for disturbance amplitudes $u'/U_e < 1{\cdot}5$ %. (See, for example, table 3-1 in Strazisar 1975.) Further proof of the small amplitude nature of the artificial disturbance is provided by the fact that the ribbon vibration has no measurable effect on the mean velocity and temperature profiles. It should be noted at this point that the 3 Hz window width of the wave analyser is used to measure the disturbance amplitude at all frequencies. This practice assumes that the width of the spectral peak associated with the artificial disturbance is independent of the disturbance frequency and flow conditions, so that the same amount of signal falls within the 3 Hz window at all times.

The development of ribbon-generated disturbances just downstream of the ribbon is investigated to ensure that the disturbances develop fully before reaching the station where growth rates are first measured, namely $\bar{x} = 5$ in. Figure 5 shows the results for a decaying disturbance with $\omega_r = 138 \times 10^{-6}$ and $Re = 601$ at $\bar{x} = 5{\cdot}5$ in. (The lower-branch neutral point obtained experimentally at $Re = 601$ is at $\omega_r = 150 \times 10^{-6}$.) Points in figure 5 in the region $\eta < 0{\cdot}75$ are shown as broken symbols owing to the

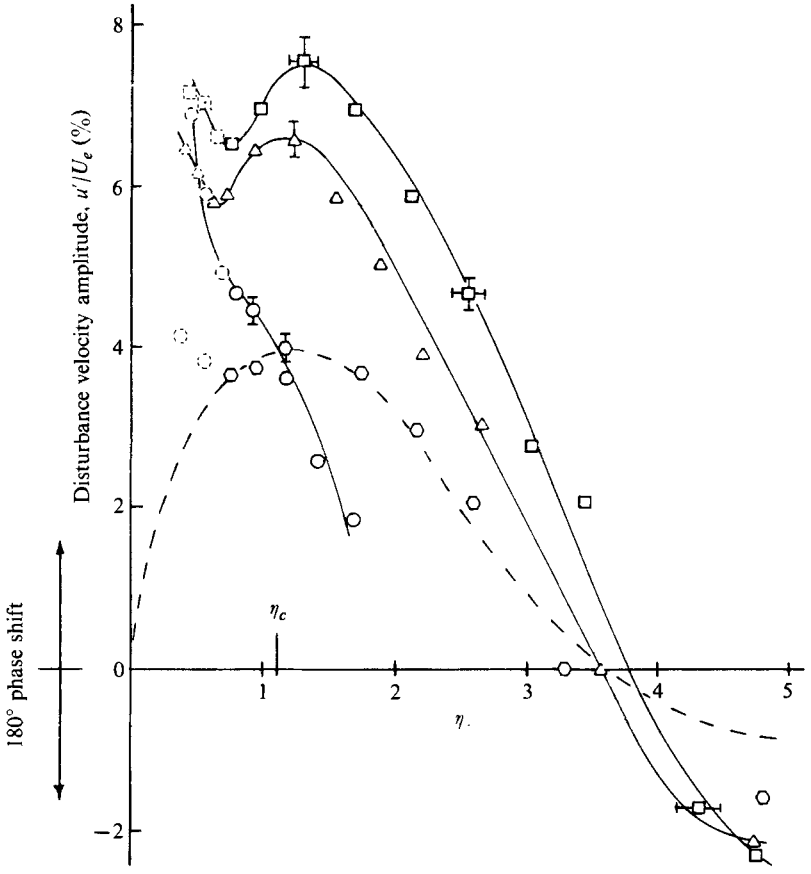

FIGURE 5. Development of the velocity disturbance amplitude distribution downstream of the ribbon. Ribbon at $\bar{x} = 3{\cdot}75$ in., $\bar{T}_w - \bar{T}_\infty = 0\,°\text{F}$, $\bar{T}_\infty = 75\,°\text{F}$, $\bar{\lambda} = 0{\cdot}656$ in., $\omega_r \times 10^6 = 138$. ○, $\bar{x} = 4$ in.; □, $\bar{x} = 4{\cdot}5$ in.; △, $\bar{x} = 5{\cdot}0$ in.; ⬡, $\bar{x} = 5{\cdot}5$ in.; – – –, solution by Lowell (1974) for $Re = 601$, corresponding to $\bar{x} = 5{\cdot}5$ in.; ——, smooth curves drawn through the data points.

possible wall interference effects discussed in § 4 above. The disturbance amplitude distribution through the boundary layer attains its final shape at $\bar{x} = 4{\cdot}5$ in. but the peak amplitude increases between $\bar{x} = 4{\cdot}0$ in. and $\bar{x} = 4{\cdot}5$ in. Downstream of $\bar{x} = 4{\cdot}5$ in. both the shape and the peak amplitude of the distribution display the proper behaviour. Figure 5 thus illustrates that the proper growth behaviour begins once the eigenfunction has attained the proper shape. The distance required for the eigenfunction development in this case is twelve boundary-layer thicknesses (or 1·2 wavelengths based on the measured value of $\bar{\lambda} = 0{\cdot}656$ in.).

The disturbance amplitude distribution calculated from Lowell's (1974) program for $Re = 601$ is also shown in figure 5. Since Lowell's results are independent of any scale factor, the calculated distribution is scaled to the measured distribution by equating the areas under the distributions between $\eta = 0{\cdot}75$ and the value of η at which $u'/U_e = 0$. The measured disturbance amplitude distribution displays good qualitative agreement with the numerical result. In particular, the phase shift of 180° occurs in the region $3 < \eta < 4$ and the peak amplitude occurs near the critical point η_c. Further measurements indicate that the shape of the amplitude distribution is fairly inde-

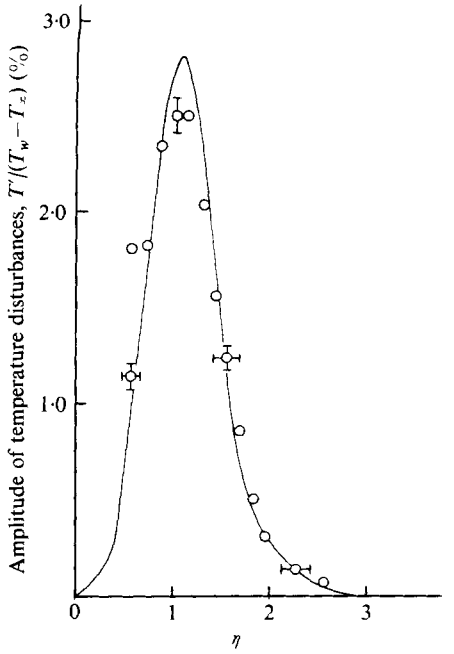

FIGURE 6. Comparison between theoretical and measured temperature disturbance amplitude distributions. ——, solution by Lowell (1974) for $Re = 890$, $\bar{T}_w - \bar{T}_\infty = 5\,°\mathrm{F}$, $\bar{T}_\infty = 75\,°\mathrm{F}$, $\omega_r \times 10^6 = 81$; ○, data for $Re = 890$, $\bar{T}_w - \bar{T}_\infty = 5{\cdot}2 \pm 0{\cdot}1\,°\mathrm{F}$, $\bar{T}_\infty = 75\,°\mathrm{F}$, $\omega_r \times 10^6 = 83$.

pendent of disturbance frequency at a fixed Re in both the heated and the unheated boundary layer.

A measured disturbance temperature amplitude distribution is compared with the corresponding numerical solution in figure 6. The calculated distribution is scaled by equating the areas under the measured and calculated distributions in the region $0{\cdot}75 < \eta < 3$. The shape of the disturbance temperature amplitude distribution is also found to be virtually independent of the disturbance frequency at a fixed Re.

6. Unheated stability results

As described in § 3.3, upper- and lower-branch neutral points are determined from plots of α_i *vs.* ω_r at a fixed Re. One such plot is shown in figure 7, where the experimental results are compared with the numerical results for parallel and non-parallel flow of Saric (1976, private communication).† The parallel-flow results of Saric (1976) are identical to those of Jordinson (1970) and to the unheated results of Wazzan *et al.* (1970) and Lowell (1974). The measured growth rates are seen to be in closer agreement with the non-parallel-flow than with the parallel-flow prediction. The agreement between experimental results and numerical results for non-parallel flow shown here is typical of results obtained at $Re < 800$.

Neutral points found in the present investigation are compared with previous

† The authors wish to thank Dr William Saric of Virginia Polytechnic Institute and State University for providing them with more detailed numerical results than those available in the paper by Saric & Nayfeh (1975).

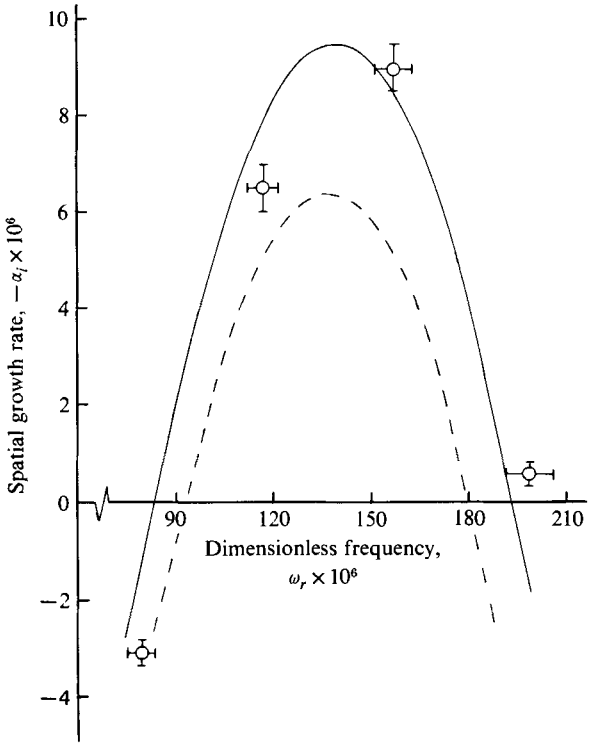

FIGURE 7. Comparison between theoretical and measured spatial growth characteristics for the unheated boundary layer at $Re = 764$. ——, non-parallel flow, Saric (1976); – – –, parallel flow, Saric (1976); ○, experiment.

experimental results and with Saric & Nayfeh's (1975) numerical results in figure 8. Lower-branch neutral points in the region $Re < 500$, $\omega_r > 210 \times 10^{-6}$ are denoted by bars because distinct neutral points could not be identified. Experimental results indicate that a neutral point lies somewhere in the barred region at each disturbance frequency considered.

The difficulty which arises in determining lower-branch neutral points at high values of ω_r is due to the fact that the decay rate of a high frequency disturbance for Re less than the lower-branch Re is much smaller than its decay rate for Re greater than the upper-branch Re. This behaviour is shown by Saric's (1976) results for non-parallel flow (figure 9) and has also been found in the stability analysis of Fasel (1974) using the full Navier–Stokes equations.

The present neutral results in figure 8 are in agreement with previous experimental results and provide further verification of the departure from parallel-flow solutions in the region $Re < 500$. This departure is evidently due to a gradual breakdown in the parallel-flow assumption as the Reynolds number decreases. A measure of this effect is provided by the parameter λ/l_c, where $\bar{\lambda}$ is the disturbance wavelength and $\bar{l}_c$ is a length which characterizes the distance over which the mean flow changes owing to non-parallel effects ($\bar{l}_c^{-1} = \bar{\delta}^{-1}\, d\bar{\delta}/dx$). The value of λ/l_c in the present work in the region $Re \doteq 400$–450 is 7–9 %, and the parallel-flow assumption $\lambda/l_c \ll 1$ may be questionable at these Reynolds numbers.

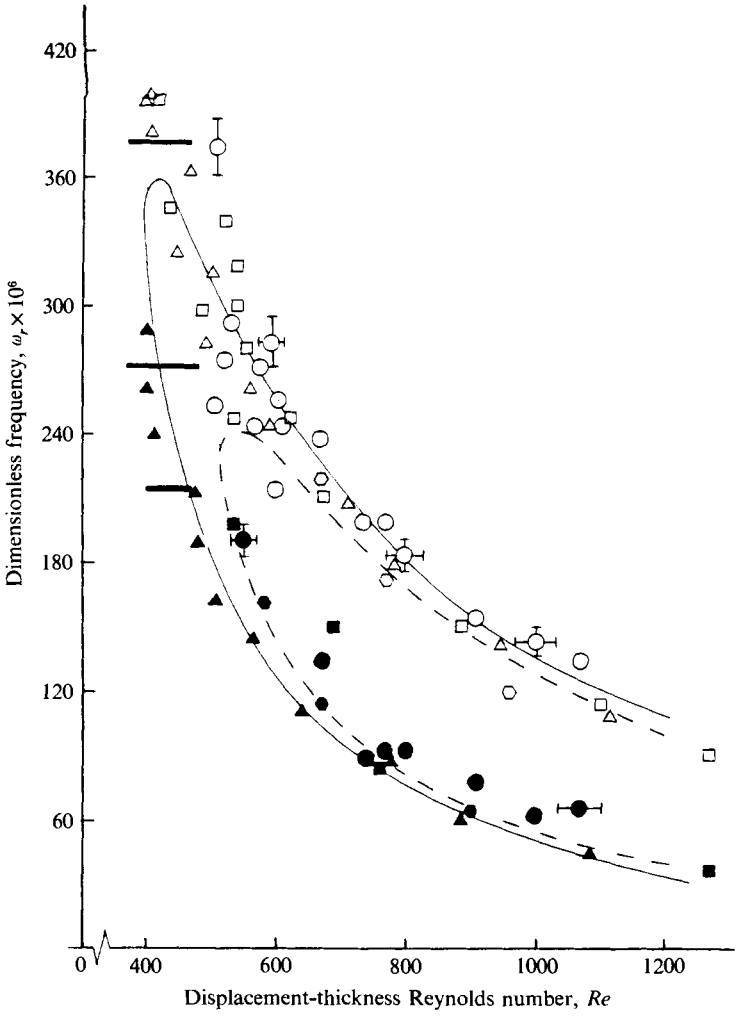

FIGURE 8. Comparison of unheated neutral points with results of previous investigations. ——, non-parallel flow, Saric (1976); – – –, parallel flow, Saric (1976); △, Ross *et al.*; □, Schubauer & Skramstad; ○, Wortmann; □, ○, present study. Solid symbols, lower branch; open symbols, upper branch.

Points of neutral amplification in the α_r, Re and c_r, Re planes are compared with previous experimental results and with the solutions of Saric (1976) in figure 10. The present results indicate neutral values of α_r and c_r which are in general agreement with previous results at a given Re. There is a consistent trend in all experimental results towards neutral values of α_r and c_r at Reynolds numbers below the parallel-flow value of $Re_{c\,\min} = 520$, in agreement with the non-parallel-flow solution. Agreement between theory and experiment for upper-branch neutral points is generally improved by using the non-parallel-flow formulation.

The departure from parallel-flow theory at low values of Re is not confined to neutral results but appears in disturbance growth rates as well. Experimental results for the maximum growth rate at a fixed Re are compared with Saric's (1976) numerical results in figure 11. The points attributed to Ross *et al.* (1970) are obtained by differentiating

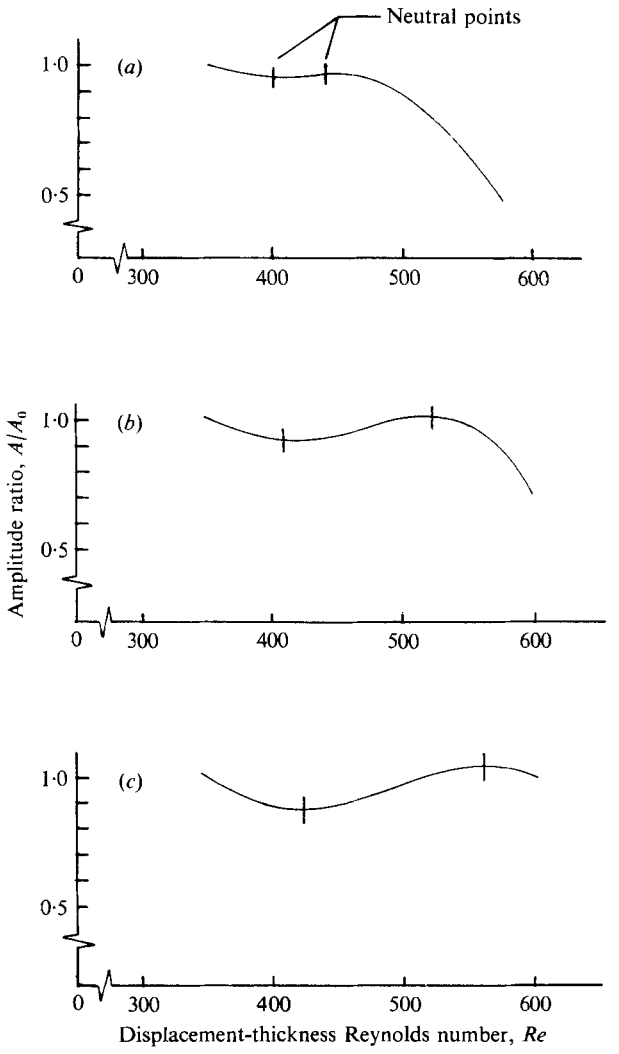

FIGURE 9. Disturbance amplitude *vs.* Reynolds number for a fixed disturbance frequency. $A/A_0 = 1$ at $Re = 350$. Calculation of Saric (1976). (*a*) $\omega_r = 350 \times 10^{-6}$. (*b*) $\omega_r = 300 \times 10^{-6}$. (*c*) $\omega_r = 275 \times 10^{-6}$.

a plot of $\ln A/A_0$ *vs.* $\int \alpha_i dx$ with respect to x while the point attributed to Schubauer & Skramstad (1948) is converted from a temporal to a spatial growth rate by using the group velocity. The trend of the experimental results towards decreasing values of $(-\alpha_i)_{\max}$ for $Re > 800$ does not agree with the numerical results. However at Reynolds numbers nearest the minimum critical value the measured growth rates do tend to be higher than those predicted by parallel-flow theory.

Note that, although the difference between predictions of $(-\alpha_i)_{\max}$ for parallel and non-parallel flow increases for $Re < 800$, the disturbance frequencies associated with the maximum growth rates in this region are relatively high. The increased growth rates predicted by results for non-parallel flow are therefore not 'dangerous' in the sense of causing transition. The maximum value of $-\alpha_i$ for non-parallel flow is approximately $9{\cdot}55 \times 10^{-6}$ and occurs at $Re = 795$, $\omega_r = 135 \times 10^{-6}$. The total growth

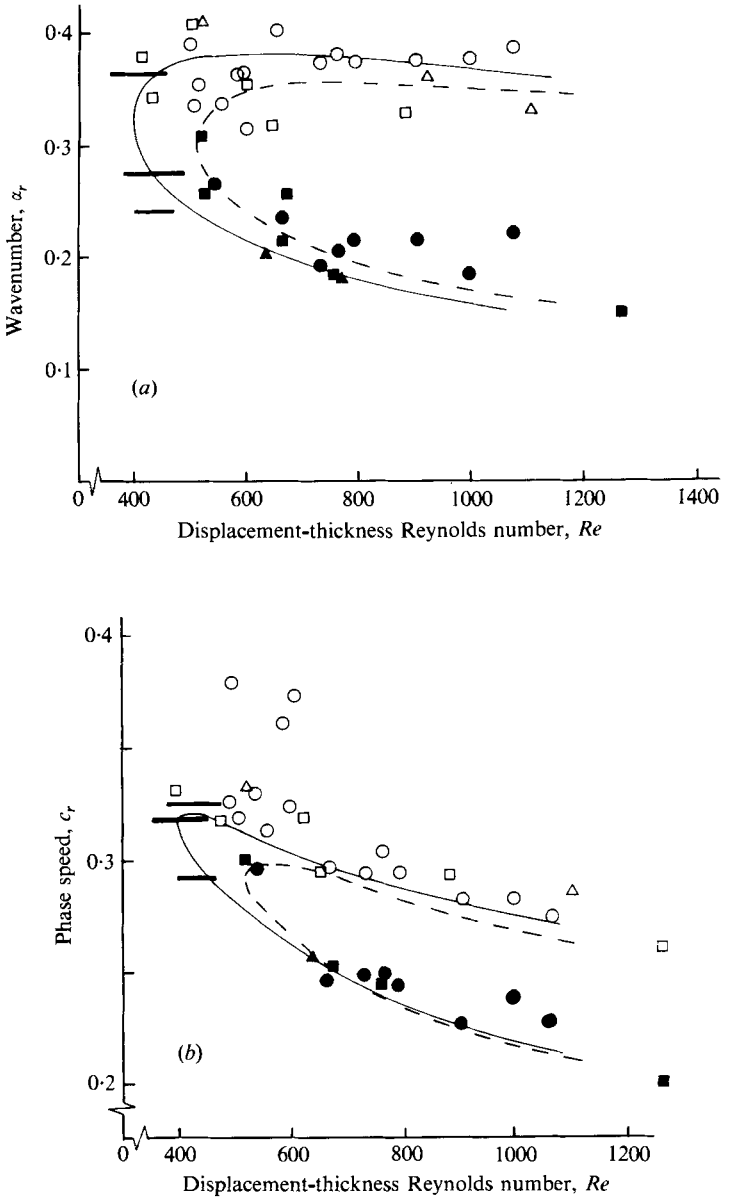

FIGURE 10. Comparison of unheated neutral points with results of previous investigations (*a*) for wavenumber and (*b*) for phase speed. ——, non-parallel flow, Saric (1976); – – –, parallel flow, Saric (1976); △, Ross *et al.*; □, Schubauer & Skramstad, ▭, ○, present study. Solid symbols, lower branch; open symbols, upper branch.

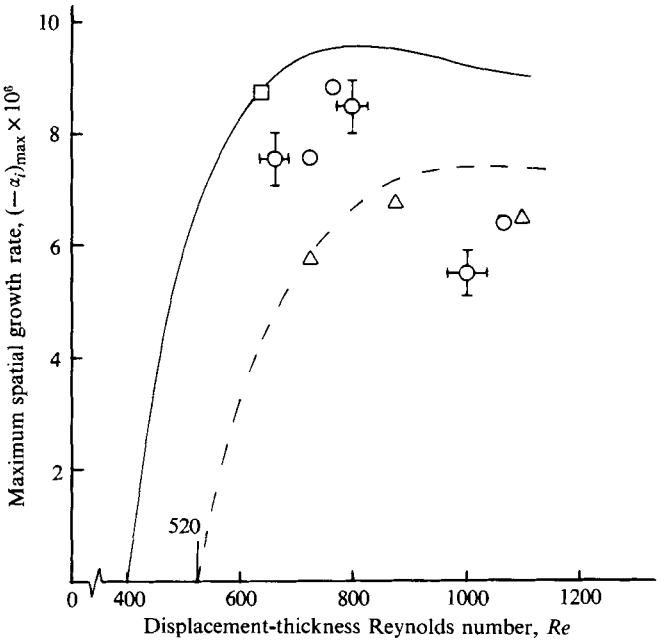

FIGURE 11. Comparison between theoretical and measured maximum spatial growth rate for a fixed Re, unheated. ——, non-parallel flow, Saric (1976); – – –, parallel flow, Saric (1976); △, Ross *et al.*; □, Schubauer & Skramstad; ○, present study.

of a disturbance with $\omega_r = 135 \times 10^{-6}$ between the lower and upper branch of the neutral curve for non-parallel flow is

$$\ln A/A_0 = \frac{2}{(1{\cdot}7208)^2} \int_{Re_l}^{Re_u} -\alpha_i Re dRe = 2{\cdot}11,$$

which is well below the range of values (say $\ln A/A_0 \approx 9$) generally identified with transition.

The unheated stability results presented above serve as a test of equipment and procedures. Since the results are in agreement with previous experimental results, they form a proper basis for comparison with stability characteristics determined for heated cases, $\bar{T}_w - \bar{T}_\infty > 0$. Since no numerical investigation of effects of non-parallel flow on the heated boundary layer has been performed to date, the parallel-flow solutions of Lowell (1974) are used for comparison with theory.

7. Heated stability results

Curves of neutral amplification for increasing values of $\bar{T}_w - \bar{T}_\infty$ obtained from Lowell's (1974) program are shown in figure 12. The main features of these results as $\bar{T}_w - \bar{T}_\infty$ increases are as follows.

(i) The increase in $Re_{c\,\min}$.

(ii) The decreased range of frequencies which receive amplification.

(iii) The nesting of neutral curves within one another.

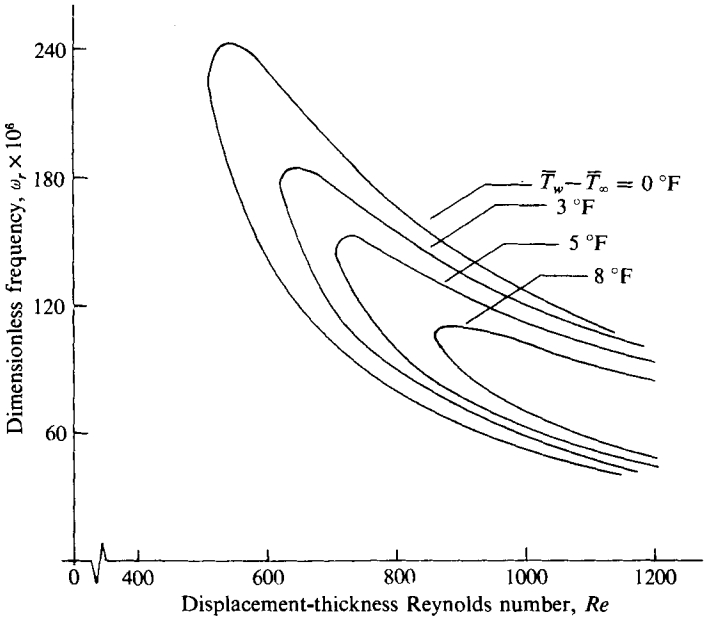

FIGURE 12. Parallel-flow neutral curves for varying wall temperature calculated by Lowell (1974) for $\bar{T}_\infty = 75$ °F.

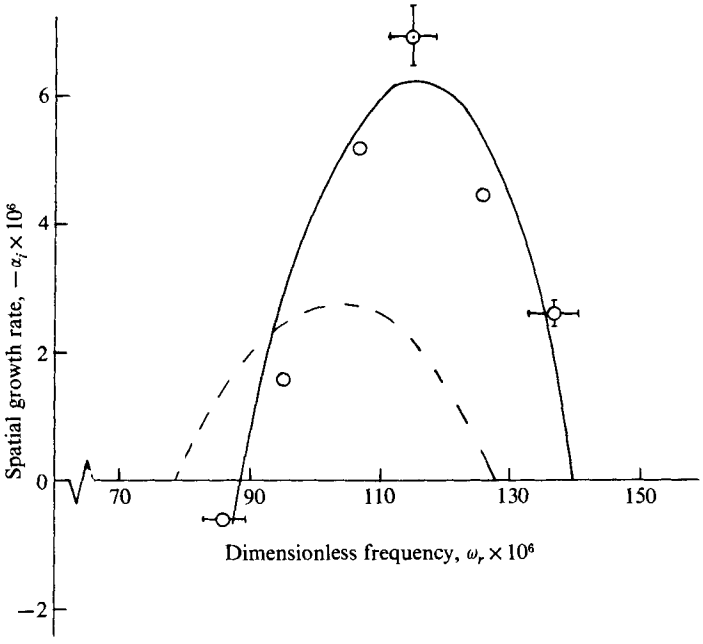

FIGURE 13. Comparison between theoretical and measured spatial growth characteristics for the heated boundary layer at $Re = 910$. – – –, parallel-flow solution by Lowell (1974) for $\bar{T}_w - \bar{T}_\infty = 5$ °F, $\bar{T}_\infty = 75$ °F; ○, experiment for $\bar{T}_w - \bar{T}_\infty = 5{\cdot}4 \pm 0{\cdot}35$ °F, $\bar{T}_\infty = 75{\cdot}1$ °F; ——, smooth curve drawn through the data points.

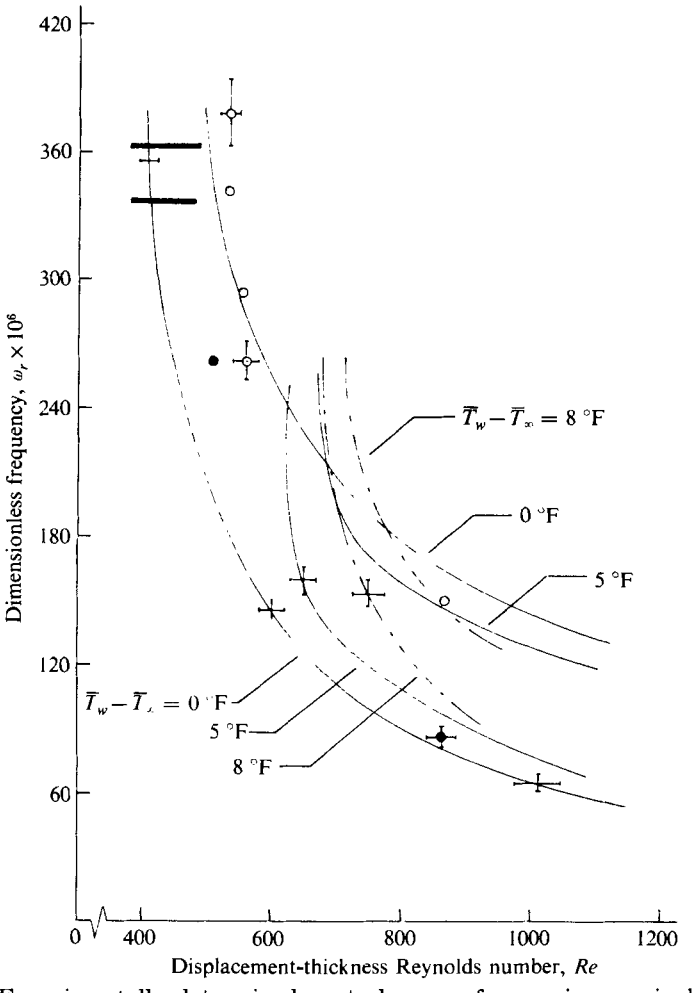

FIGURE 14. Experimentally determined neutral curves for varying nominal wall temperature; $\overline{T}_\infty = 75$ °F. □, ○, neutral points for $\overline{T}_w - \overline{T}_\infty = 3{\cdot}4 \pm 0{\cdot}1$ °F, $\overline{T}_\infty = 75$ °F. Solid symbols, lower branch; open symbols, upper branch.

A comparison between predicted and measured growth rates at $Re = 910$ for a nominal $\overline{T}_w - \overline{T}_\infty$ of 5 °F is shown in figure 13, where the solid line is a smooth curve drawn through the measured points. The shift of the measured neutral points to frequencies higher than those predicted by parallel-flow theory is consistent with the behaviour shown in figure 8 for the unheated case at the same Reynolds number. The discrepancy in growth between theory and experiment shown here suggests that the growth behaviour shown in figure 11 may prevail in the heated boundary layer. A check of all heated growth-rate measurements indicates that this is in fact true, since measured growth rates are consistently higher than those predicted by parallel-flow theory.

Figure 14 shows experimentally determined neutral curves in the ω_r, Re plane for nominal wall temperature differences of $\overline{T}_w - \overline{T}_\infty = 0$, 5 and 8 °F. The experimental neutral points associated with these wall heating levels have not been shown for the sake of clarity. The limited number of neutral points determined for $\overline{T}_w - \overline{T}_\infty = 3{\cdot}4$ °F

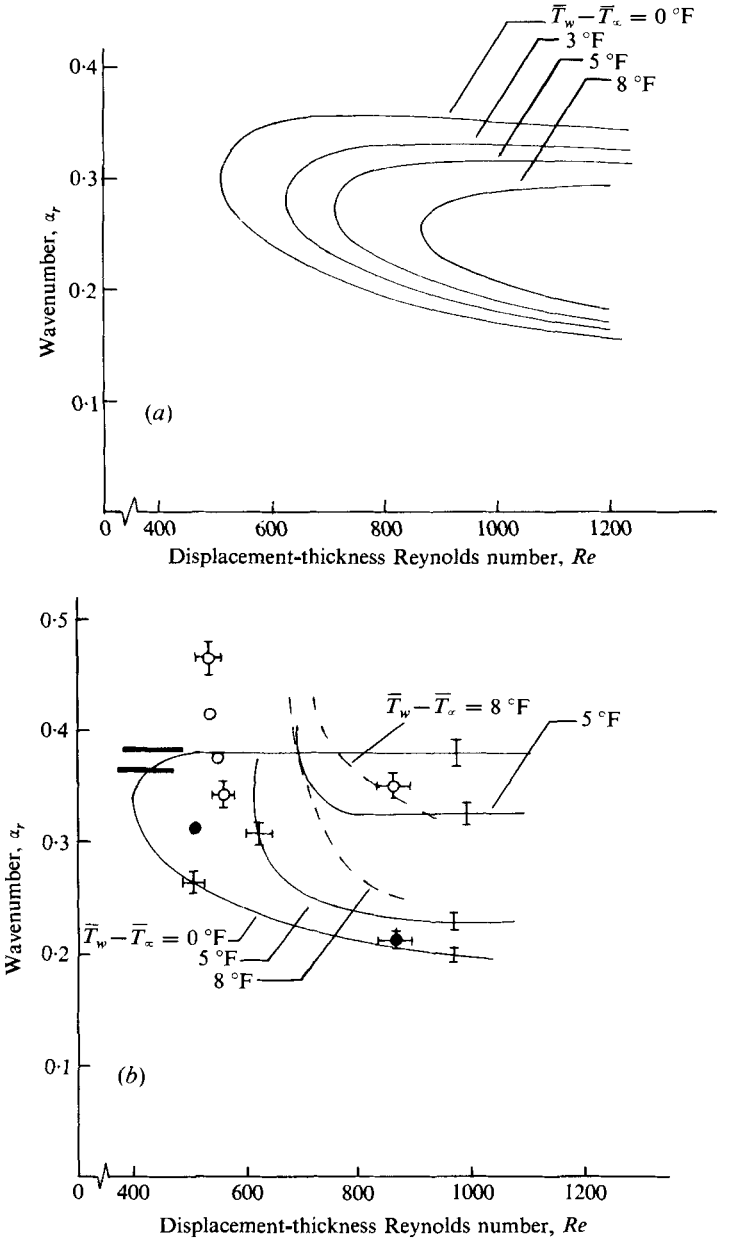

FIGURE 15. Neutral curves in the wavenumber plane for varying nominal wall temperature. (*a*) Parallel-flow solutions by Lowell (1974) for $\bar{T}_\infty = 75$ °F. (*b*) Experimental results for $\bar{T}_\infty = 75$ °F. □, ○, neutral points for $\bar{T}_w - \bar{T}_\infty = 3{\cdot}4 \pm 0{\cdot}1$ °F, $\bar{T}_\infty = 75$ °F. Solid symbols, lower branch; open symbols, upper branch.

are shown in figure 14. Comparison of figures 12 and 14 indicates that the difference between experimental and numerical results found near $Re_{c\,\min}$ for the unheated case persists in the heated cases. Trends in the experimental results which agree with those established by the numerical solutions as $\bar{T}_w - \bar{T}_\infty$ increases are the following.

(i) The increase in $Re_{c\,\min}$.

(ii) The decreased range of frequencies which are amplified.

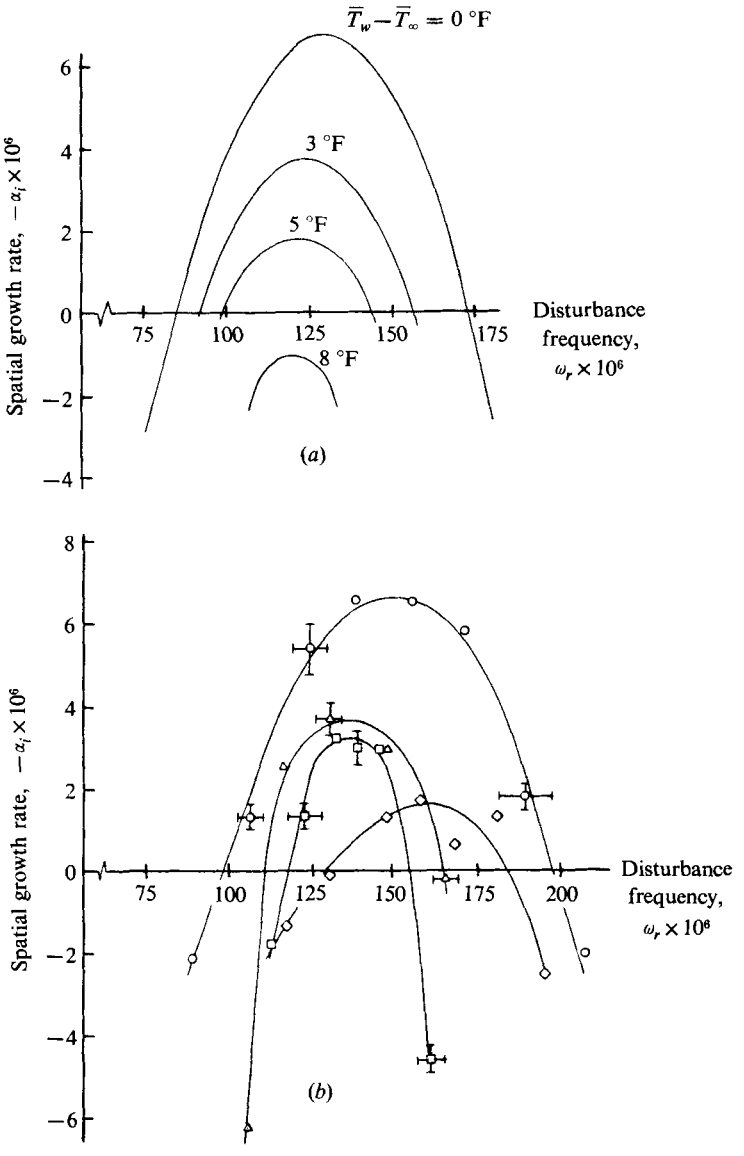

FIGURE 16. Spatial disturbance growth characteristics for varying wall temperature; $Re = 800$. (*a*) Parallel-flow solutions by Lowell (1974) for $\bar{T}_\infty = 75$ °F. (*b*) Experimental results for $\bar{T}_\infty = 75$ °F: ○, $\bar{T}_w - \bar{T}_\infty = 0$ °F, $Re = 770$; △, $\bar{T}_w - \bar{T}_\infty = 3{\cdot}15 \pm 0{\cdot}11$ °F, $Re = 781$; □, $\bar{T}_w - \bar{T}_\infty = 4{\cdot}97 \pm 0{\cdot}33$ °F, $Re = 773$; ◇, $\bar{T}_w - \bar{T}_\infty = 8{\cdot}87 \pm 0{\cdot}61$ °F, $Re = 781$; ——, smooth curve drawn through the data points.

Note that the neutral curves are not nested within one another for increasing values of $\bar{T}_w - \bar{T}_\infty$ until the Reynolds number is higher than 860.

Neutral curves in the α_r, Re plane obtained experimentally are compared with those calculated from Lowell's (1974) program in figure 15. Neutral values of α_r measured experimentally are consistently higher than the predicted values at a given Reynolds number.

Predicted and measured growth-rate characteristics are shown in figure 16 for

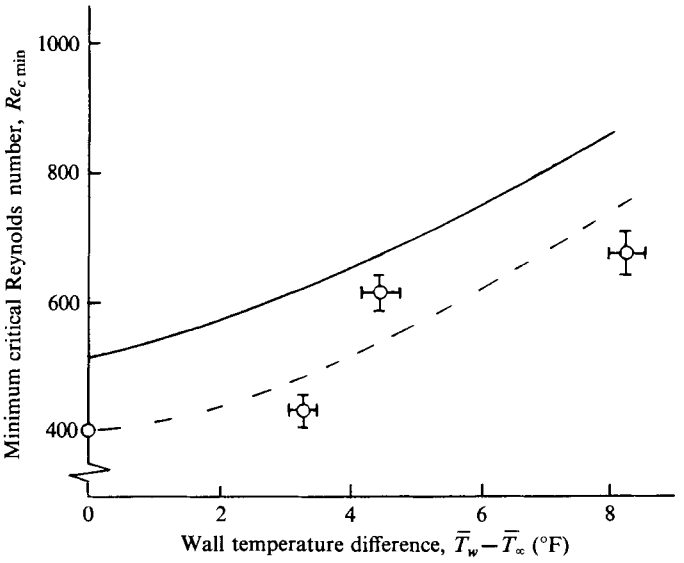

FIGURE 17. Comparison between theory and experiment for the increase in $Re_{c\,\min}$ with wall heating. ——, solution of Lowell (1974); ○, experiment; – – –, smooth curve drawn through the data points.

Re = 770–780. In this particular range of Reynolds numbers the experimental results of figure 14 show that the neutral curves are nested within one another as $\overline{T}_w - \overline{T}_\infty$ increases up to the value $\overline{T}_w - \overline{T}_\infty \approx 5$ °F. Figure 16(*a*) shows that the predicted maximum growth rate and the bandwidth of frequencies receiving amplification both decrease monotonically as the level of wall heating increases. Figure 16(*b*) shows that the measured value of $(-\alpha_i)_{\max}$ does not decrease as rapidly as predicted by parallel-flow theory. These results further suggest that the growth behaviour shown in figure 11 prevails in the heated boundary layer.

Predicted and measured values of $Re_{c\,\min}$ for various degrees of wall heating are compared in figure 17. The measured rate of increase in $Re_{c\,\min}$ compares favourably with that predicted by Lowell (1974) and Wazzan *et al.* (1970). Over the range of values of $\overline{T}_w - \overline{T}_\infty$ covered by the present work it is conjectured that the non-parallel nature of the Blasius boundary layer acts to reduce the value of $Re_{c\,\min}$ predicted from parallel-flow analyses by an amount which is independent of the level of wall heating.

8. Conclusions

A detailed exploration has been made of the growth characteristics of small amplitude disturbances in a boundary layer developing over a heated flat plate of uniform surface temperature. The results verify that wall heating in water delays the onset of growth of Tollmien–Schlichting disturbances. Trends in the results are consistent with predictions from numerical analyses. As wall heating is increased there is

(i) an increase in $Re_{c\,\min}$,

(ii) a decrease in disturbance growth rates,

(iii) a decreased band of unstable disturbance frequencies and wavenumbers.

The discrepancy with parallel-flow theory observed by previous investigators for the

unheated boundary layer near $Re_{c\,\min}$ is found to persist in the heated cases. Amplified disturbances are found at Reynolds numbers below the predicted $Re_{c\,\min}$, accompanied by an increasing discrepancy between predicted and measured growth rates as $Re_{c\,\min}$ is approached. In this region non-parallel-flow analysis displays adequate accuracy and the disturbance growth rates have been shown to be 'non-dangerous' in the sense of causing transition. The present experimental results suggest the need for non-parallel-flow analysis of stability problems involving boundary-layer control mechanisms such as wall heating, pressure gradients and suction.

The authors wish to acknowledge the important contributions of Dr Minor Nice to reconstructing and improving the water-tunnel facility and to developing the measurement techniques used in the present work. The support of this work by the Office of Naval Research is gratefully acknowledged.

REFERENCES

BOUTHIER, M. 1972 *J. Méc.* **11**, 599.

BOUTHIER, M. 1973 *J. Méc.* **12**, 75.

FASEL, H. 1974 Untersuchungen zum Problem des Grenzschichtumschlages durch numerische Integration der Navier–Stokes–Gleichungen. Ph.D. dissertation, University of Stuttgart.

GASTER, M. 1974 *J. Fluid Mech.* **66**, 465.

JORDINSON, R. 1970 *J. Fluid Mech.* **43**, 801.

LOWELL, R. S. 1974† Numerical study of the stability of a heated water boundary layer. Ph.D. dissertation, Case Western Reserve University. (See also *Dept. Fluid, Thermal Aerospace Sci., Case Western Reserve Univ. Rep.* FTAS/TR-73-93.)

NICE, M. 1973† Experimental study of the stability of a laminar boundary layer in water. Ph.D. dissertation, Case Western Reserve University. (See also *Dept. Fluid, Thermal Aerospace Sci., Case Western Reserve Univ. Rep.* FTAS/TR-73-90.)

ROSS, J. A., BARNES, F. H., BURNS, J. G. & ROSS, M. A. S. 1970 *J. Fluid Mech.* **43**, 819.

SARIC, W. & NAYFEH, A. 1975 *Phys. Fluids* **18**, 945.

SCHLICHTING, H. 1968 *Boundary-Layer Theory*, 6th edn. McGraw-Hill.

SCHUBAUER, G. B. & SKRAMSTAD, H. K. 1948 *N.A.C.A. Rep.* no. 909.

STRAZISAR, A. J. 1975† Experimental study of the stability of heated laminar boundary layers in water. Ph.D. dissertation, Case Western Reserve University. (See also *Dept. Fluid, Thermal Aerospace Sci., Case Western Reserve Univ. Rep.* FTAS/TR-75-113.)

TAN-ATICHAT, J., NAGIB, H. M. & PLUISTER, J. W. 1973 *Proc. 3rd Symp. Turbulence in Liquids, Univ. Missouri, Rolla.*

WAZZAN, A. R., OKAMURA, T. T. & SMITH, A. M. O. 1968 *J. Heat Transfer* **90**, 109.

WAZZAN, A. R., OKAMURA, T. T. & SMITH, A. M. O. 1970 *Proc. 4th Int. Heat Transfer Conf.* (ed. U. Grigull & E. Hahne). Elsevier.

WORTMANN, F. X. 1955 50 *Jahre Grenzschichtforschung* (ed. H. Goertler & W. Tollmien), p. 460. Braunschweig: Vieweg.

† Also available through Ann Arbor Microfilms.